Snake like light beam propagation in Multimode Periodic Segmented Waveguide

Pierre Aschieri, Valérie Doya

Snake like light beam propagation in Multimode Periodic Segmented Waveguide

Pierre Aschiéri[1,*] and Valérie Doya[1]

[1] *Univ. Nice Sophia Antipolis, CNRS, LPMC, UMR 7336, 06100 Nice, France*

(Dated: October 17, 2013)

Abstract

In this article it is shown that for specific initial conditions an input beam injected in a Multimode Periodic Segmented Waveguides (MPSW) does not diffract and remains collimated all along the waveguide whereas a speckle like pattern is expected at the output of a multimode structure. This nonintuitive behavior can be explained with the help of ray and wave chaos properties. A modal analysis developed in this article reveals that this nondiffractive beam regime is due to a specific superposition of modes with regularly spaced propagation constants. A discrepancy with the commonly used Equivalent Continuous Waveguide model (ECWG) is also identified.

OCIS codes: (130.2790) Guided waves,(230.7370) Waveguides,(190.3100) Instabilities and chaos

http://dx.doi.org/10.1364/XX.99.099999

* pierre.aschieri@unice.fr

1. Introduction

A Periodic Segmented Waveguide (PSW) is characterized by an array of high refractive index regions in a low refractive index substrate along the direction of propagation. It has been shown that this kind of waveguides exhibits several interesting properties for many practical purpose. They have been used in linear applications to make tapers or mode filters [1–8], exploiting the fact that the mode size and the propagation constant can be adjusted by varying the duty-cycle (defined as the ratio of the high index segment over the period Λ_{PSW}). Elsewhere, these waveguides have been used to achieve efficient nonlinear guided wave interaction using the Quasi Phase Matching (QPM) or Balanced Phase Matching (BPM) schemes [9–11] that take advantage of a periodic reversal of the nonlinear coefficient associated with such waveguides. PSW also exhibits interesting properties that can be useful for optical power managing applications [12]. More recently, MPSW have been proved to be responsible for the emergence of a genuine chaotic behavior of rays [13, 14]. In many optical systems such as asymmetric optical billiards, deformed microcavities or corrugated waveguides [15–27], ray chaos comes from the waveguide geometry, for MPSW that we consider here, ray chaos comes from the waveguide geometry characterized by a longitudinal periodic modulation (segmentation) and by the transverse index profile characterized by a Gaussian index profile (non harmonic). Light propagation in MPSW can then be described by a nonlinear Mathieu-like equation which is intrinsically chaotic. The geometrical approach of light propagation in MPSW reveals complex Poincaré sections associated to a typical mixed dynamics [13] where stable and chaotic regions coexist. The extension of the analysis of the system to the wave domain leads that what is commonly called the *wave chaos* which is devoted to the study of wave motion when the geometrical limit of rays is chaotic. Imprints of ray chaos may be found on spatial properties of modes and usually shows reminiscence of the complexity of the classical Poincaré section. Thus, we have demonstrated that, depending on input illumination, an incident optical beam launched in a MPSW remains collimated all along the propagation in the waveguide if its associated trajectory is constructed on a resonance of the Poincaré section otherwise it disperses on different modes of the structure [28]. The non diffraction behavior is explained by a modal analysis which reveals that a set of particular modes with a regularly spaced constant of propagation is responsible for the beam propagation without diffraction. Moreover, it is shown that propagation constants

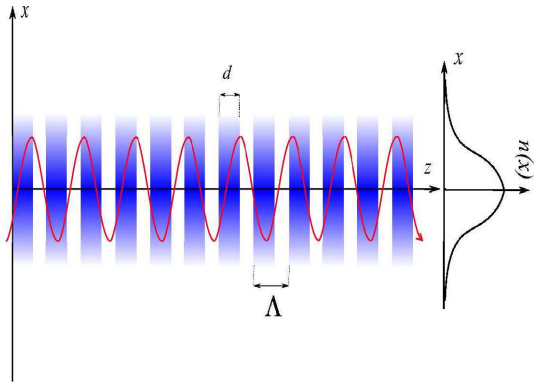

Fig. 1. Schematic of the investigated longitudinally periodic waveguide with a period Λ and the transverse gaussian index profile of the high index segments. Everywhere else, the index is constant and is equal to the substrate index n_2 and an oscillating ray path with a period of $2 \times \Lambda$.

distribution does not coincide with the one expected for the Equivalent Continuous Waveguide (ECWG) model which is commonly used for many purposes [1, 2, 6, 7, 11, 29]. The paper is organized as follows. In the next section, waveguide description is given and the geometric approach of light propagation in the system is outlined. In section 3, methods of analysis used for MPSW are briefly described, section 4 concerns numerical results of the modes analysis and wave propagation, a comparison with ECWG model is given in section 5 and finally, a conclusion is drawn in section 6.

2. Waveguide description and classical ray approach

The analysis has been developed using a 2D structure for simplicity. A typical MPSW sketched in figure 1 is formed by an array of high refractive index segments embedded in a low refractive index substrate. PSW are mostly used in a single mode configuration for practical purpose but a highly multimode structure is required to generate wave chaos. The shape of the transverse index profile of high index segments plays a key role in the ray dynamics. Previous work has shown that it has to be non-harmonic in order to generate complex rays behavior [13]. The gaussian index profile, naturally encountered with some well known waveguide fabrication technologies [30, 31] is then used for high index segments. The index profile of high index segments is given by :

$$n\left(x\right) = n_2 + \delta n e^{-\frac{x^2}{w^2}}, \tag{1}$$

where w is the width of the waveguide, $\delta n = n_1 - n_2$, n_2 is the substrate index and n_1 is the maximum refractive index value induced by the waveguide fabrication process. In low index segments, the index is constant $n(x) = n_2$. The Duty-Cycle (DC) of a PSW is commonly defined as the ratio of the length d of the high index segment over the segmentation period Λ, $DC = d/\Lambda$. A step index profile is assumed along the propagation direction z as it has been done in previous works [13, 32, 33] (a smoother profile will not change qualitatively the results). The ray path can be calculated by analyzing high and low index segments separately using the following equation [13]

$$\frac{d^2x}{dz^2} = \begin{cases} -\frac{2n_2\delta n}{\beta^2\omega^2} x e^{-\frac{x^2}{\omega^2}} & ; (p-1)\Lambda \leq z \leq (DC+p-1)\Lambda \\ 0 & ; (DC+p-1)\Lambda < z < p\Lambda \end{cases} \tag{2}$$

where p is the segment number, $\beta = n(x_0)\cos\theta_0$ is the invariant of the ray path, x_0 being the initial position of the ray and θ_0 being the incident angle of the ray respect to z axis [34]. Equation (2) is periodic with z and nonlinear respect to x, it is a nonlinear Mathieu-like equation, then it may exhibits nonlinear resonances, frequency locking, as well as a chaotic behavior as will be seen subsequently. It has to be mentioned that the dynamics of a such system is comparable to an undamped nonlinear pendulum forced by a periodic motion of the suspension point. A typical ray trajectory is superimposed on the waveguide sketched in figure 2 and the corresponding Poincaré section is given in figure 2 (a). Poincaré section is constructed by a projection of the trajectory (x, θ, z) onto the phase plane (x, θ) at positions $z = n\Lambda$, $n = 1, 2, 3, ...$ for an ensemble of various initial conditions. Non diverging trajectories are constructed on KAM (Kolmogorov-Arnold-Moser) torus characterized by close curve circle whereas diverging trajectories are represented by dots. Waveguides parameters are chosen so that the ray dynamics exhibits interesting feature. For example, the ray trajectory in figure 1 is oscillating with a period of $2 \times \Lambda$ and refers to resonances in which the period of the trajectory is synchronized with the period of the segmentation. Resonances of the system can be clearly identified with the help of Poincaré section as it is shown in figure 2 (a) where the two stable resonances are surrounded by a chaotic sea represented by dots. Resonances generate stable periodic trajectories while rays that belong to the chaotic sea exhibit ergodic trajectories. The coexistence of regular and chaotic regions on the Poincaré section is the signature of a mixed dynamics. An other waveguide configuration leads to a different Poincaré section as it can be seen with figure (2) (b) which exhibits a central main

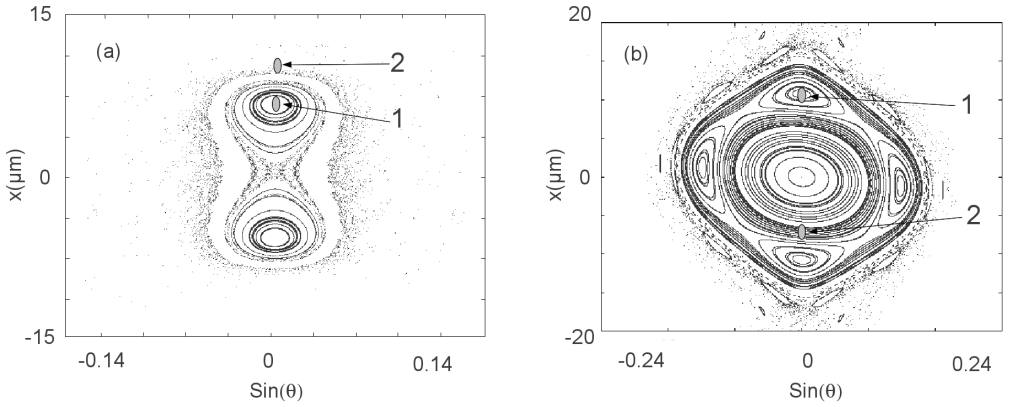

Fig. 2. Poincaré section of the waveguide that exhibits 2 resonances surrounded by a chaotic sea (a). Waveguide parameters are $\delta n = 0.024$, $\Lambda = 300\mu m$, the waveguide width is $w = 12.3\mu m$ and the $DC = 0.8$. Poincaré section for a different waveguide configuration that exhibits 4 peripheral resonances surrounded by closed curves corresponding to stable trajectories (b). Waveguide parameters are $\delta n = 0.05$, $\Lambda = 146\mu m$, the waveguide width is $w = 15\mu m$ and the $DC = 0.8$.

resonance surrounded by 4 peripheral resonances and KAM torus.

3. Numerical modal analysis

In this section, we extend our analysis to the wave domain and we briefly outline useful methods which help to get a better insight into effects involved in light wave propagation in MPSW. Light propagation in a MPSW can be described by the scalar Helmholtz equation :

$$\Delta\Psi + k_0 n^2(x,z)\Psi = 0 \tag{3}$$

where Ψ is the e.m. field, $k_0 = 2\pi/\lambda$, $n(x, z+\Lambda) = n(x,z)$ and a time harmonic fields $e^{j\omega t}$ dependence is assumed. Backward propagating waves can be neglected because the index contrast $\delta n \ll 1$ and the segmentation period Λ is more than two orders of magnitude greater than the pitch of a Bragg grating [13, 32, 33, 35]. Using the classical assumptions of the slowly envelope variation and considering a TE polarization, equation (3) for the electric field E, is reduced to the parabolic wave equation :

$$2jk_0 n_0 \frac{\partial E}{\partial z} - \frac{\partial^2 E}{\partial x^2} - k_0^2 \left(n^2(x,z) - n_2^2\right) E = 0 \tag{4}$$

The transverse field evolution along the longitudinal direction is calculated using the numerical scheme FD-BPM and the propagation losses are also estimated. The propagation

constants of modes of the waveguide are computed. The classical method proposed by Feit and Fleck [36] to get fiber modes properties which has also been successfully applied to segmented waveguides [35] is used to compute propagation constants of the waveguide modes. The principle is to cross-correlate the input field $E(x,0)$ with the propagating field along the waveguide $E(x,z)$

$$c(z) = \int_{-\infty}^{+\infty} E^*(x,0)E(x,z)dx \tag{5}$$

Then, the Fourier transform of the cross correlation function :

$$C(\beta) = \int_0^L c(z)h(z)\exp\left(-i\beta z\right)dz, \tag{6}$$

where $h(z)$ is a Hanning window and L is the waveguide length, leads to the discrete modal spectrum of the waveguide where peak values are proportional to the weight of each mode actually excited by the input field. The propagating field computed by FD-BPM allows also to get Husimi [37] distribution which is widely used in wave chaos domain. Husimi distribution is the quantum wave counterpart of the classical phase space

$$\mathcal{H}(x,k) = \sum_{n=1}^{N} H(x,k,z=n\Lambda) \tag{7}$$

The Husimi distribution $\mathcal{H}(x,k)$ consists in "scanning" the optical field by a Gaussian wave packet and is defined here at periodic positions z such as $z = n\Lambda$, with $n = 1, 2, 3, ...$ The Husimi $H(x,k,z=n\Lambda)$ function for MPSW is given by :

$$H(x,k,z=n\Lambda) = \left| \frac{1}{(\pi\sigma^2)^{\frac{1}{4}}} \int_{-\infty}^{+\infty} \exp\left(ikx'\right) \exp\left(-\frac{(x'-x)^2}{2\sigma^2}\right) E(x',z)dx' \right|^2$$

where k is the wave number and σ represents the width of the scanning gaussian wave packet .

4. Numerical results

Optical wave propagation has been computed in a MPSW using FD-BPM, for all the calculations, the wavelength is set at $\lambda = 0.4\mu m$. A Gaussian input field of $1.5\mu m$-width is firstly injected such that its parameters reported in the Poincaré section coincide with a resonance (noted 1 on figure 2(a)). Secondly, it is injected outside of the resonance (noted 2 on figure 2 (a)). The intensity distribution along the waveguide, the Husimi representation and the

mode spectrum are also calculated in both cases. Results are reported in figure (3) and in figure (4). The injection of a gaussian beam located inside a resonance leads to a *snake like* beam propagation as shown in figure 3(a) whereas a spreading of the beam is expected in this multimode waveguide, and calculated propagation losses are almost zero. The beam propagation is built upon a set of oscillating rays trajectories that belong to resonances of the Poincaré section (see figure 2(a)). This is confirmed by the Husimi distribution (figure 3(b)) that exhibits 2 spots matching with the 2 main resonances of the Poincaré sections. The corresponding mode spectrum analysis (figure 3(c)) displays a set of 9 modes excited by the gaussian input. The mode spectrum shows that all the 9 modes are regularly spaced by $\Delta\beta$ which gives a beating length $L_c = \frac{\pi}{\Delta\beta} \simeq 600\mu m$ which is $2 \times \Lambda$. The factor 2 corresponds to the 2^{nd} order resonance visible in the Poincaré and Husimi representation. The beating length can also be evaluate by computing the *length spectrum* which is the fourier transform of the mode spectrum. The *length spectrum* represented on figure 3(d) exhibits only the $600\mu m$ optical path length and its harmonics. Roughly speaking, the non diffraction beam is constructed on a coherent superposition of specific modes which are periodically in phase every $600\mu m$ -eg every two segmentation period length. The input beam excitation is now modified so that it is located in the chaotic sea ((noted 2 in figure 2 (a)). The field does not remain collimated during the propagation as previously and spreads over the waveguide width as it is shown in figure 4 (a), the calculated propagation losses are $42dB/cm$. The corresponding Husimi distribution (figure 4 (b)) shows that the field is present on many spatial positions and with many direction of the wave vectors. Unlike the previous collimated beam propagation, the corresponding mode spectrum shown in figure 4(c) exhibits strong coulping with radiation modes (for $\beta < 33.57$) and a large set of modes which are no longer regularly spaced. This can also be seen by the use of the Fourier transform of the mode spectrum given by figure 4(d). For a different waveguide configuration whose Poincaré section is given in figure 2 (b), similar analysis has been performed. Figure 5 (a) correspond to an injection of the input gaussian beam in one of the 4 resonances of the system (noted 1 on figure 2(b)). Then, a *snake like* beam propagation all along the waveguide occurs. The corresponding Husimi distribution given in figure 5 (b) shows 4 spots corresponding to the 4 peripheral resonances of Poincaré section. The mode spectrum analysis (figure 5 (c)) displays a large set of modes excited by the gaussian input compared to the previous case (figure 3(c)) but they are still regularly spaced by a constant value of $\Delta\beta$. The calculated

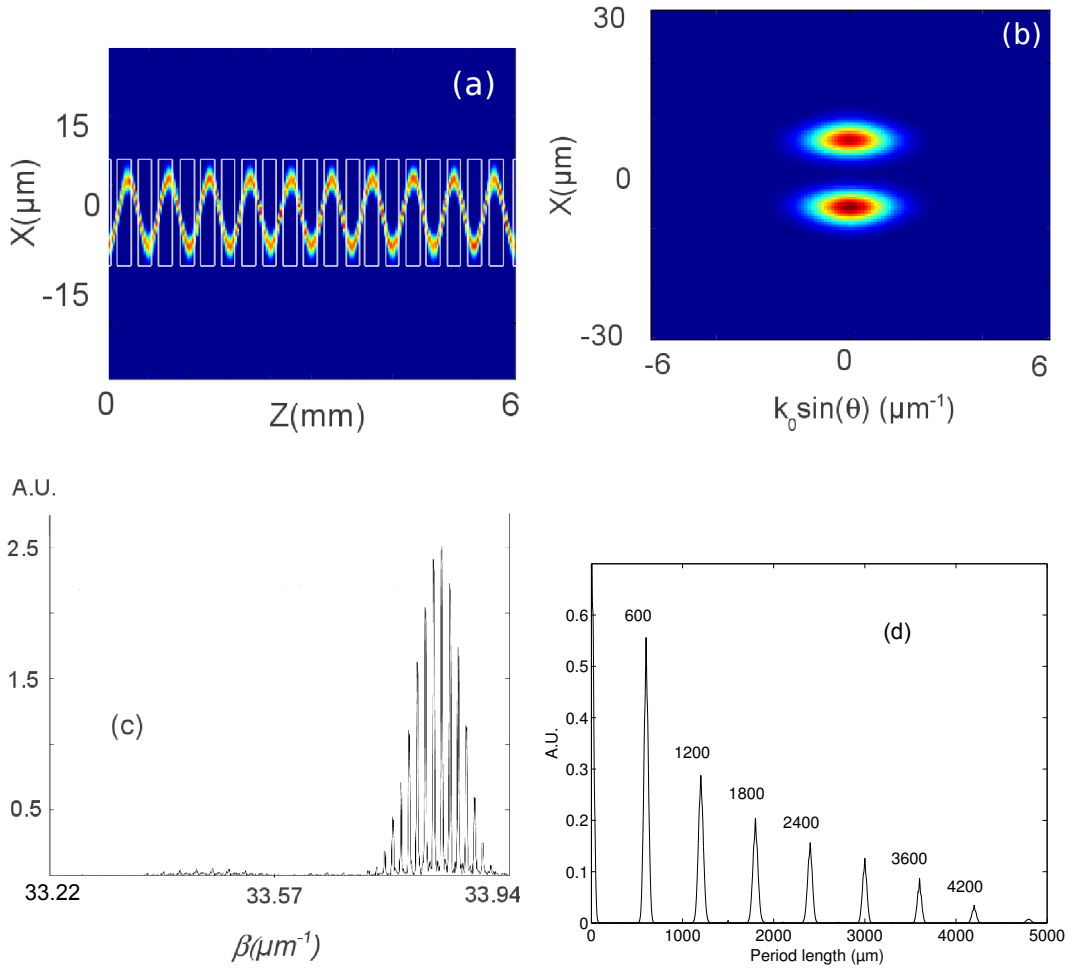

Fig. 3. Field distribution with a schematic of the waveguide segments for an incident gaussian beam launched in a resonance of the Poincaré section of the MPSW, high index segments are schematically represented by rectangles (a), Husimi representation (b). On figure (c) it is represented the modal spectrum distribution which shows that a set of modes regularly spaced are excited. The figure (d) is the length spectrum of the modal spectrum in the case of the collimated beam.

beating length gives $L_c = \frac{\pi}{\Delta\beta} \simeq 584\mu m$ which is $4 \times \Lambda$. The factor 4 now corresponds to the 4^{nd} order resonance visible in the Poincaré and Husimi representation. This beating length is confirmed by the *length spectrum* represented on figure 5(d) that exhibits only the $584\mu m$ optical path length and sub-harmonics. Like in the previous waveguide configuration, if the injection is outside the resonance (noted 2 in figure 2 (b)), the input beam is again quickly dispersed in many waveguide modes as it can be seen with figure 6 (a). The profile of the Husismi distribution (figure 6 (b)) is comparable to the shape of the main central resonance of the Poincaré section (2 (b)). The spectrum distribution and the corresponding

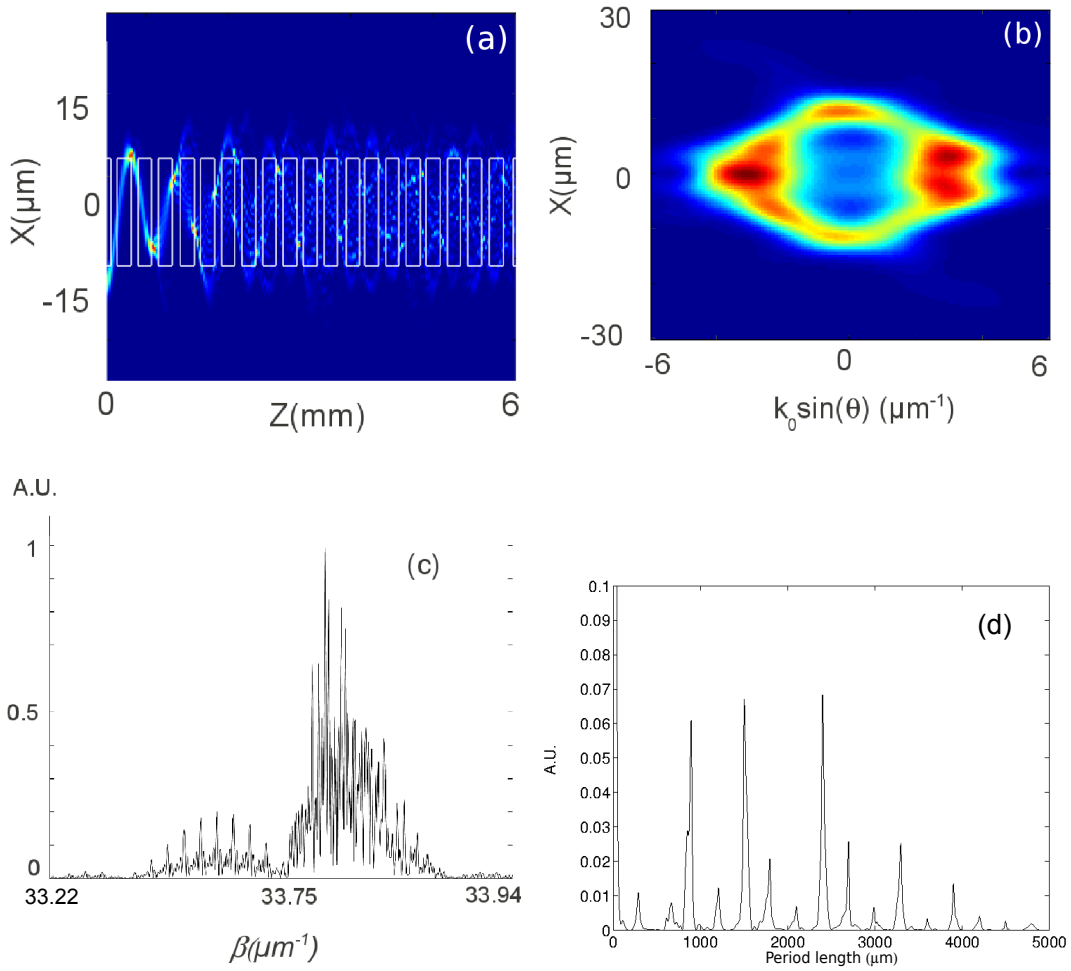

Fig. 4. Field distribution (a), Husimi representation (b) and modal spectrum (c) for an incident gaussian beam launched outside of the resonance of the Poincaré section. The field is spread on many waveguides modes which is confirmed by the Husimi distribution and the modal spectrum. The figure (d) is the corresponding length spectrum

length spectrum (figure 6 (c) and (d)) show that excited modes are not regularly spaced. In contrast, propagation losses are almost zero compared to the previous case where the beam was dispersed (figure 4 (a)), the reason is that gaussian input is in a region of the Poincaré section which is surrounded by a KAM torus which acts as a barrier that cannot be crossed by a ray trajectory and then the light remains confined in the waveguide.

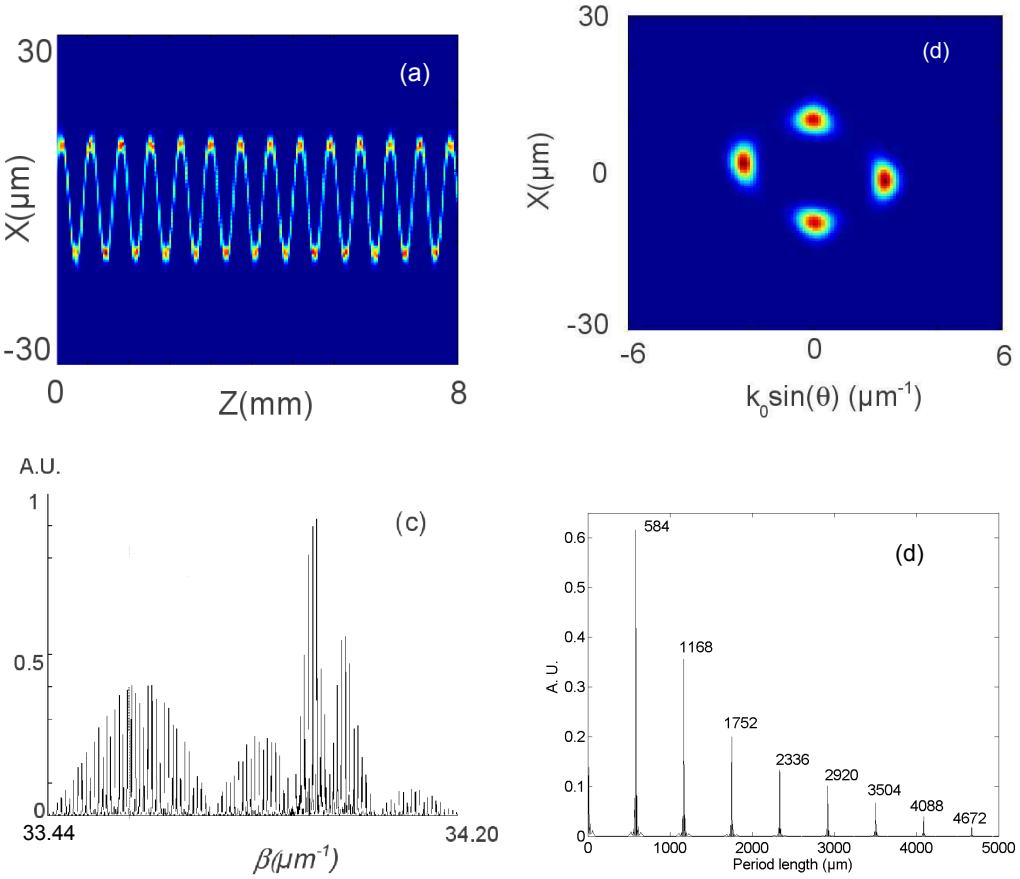

Fig. 5. Field distribution for an incident gaussin beam launched in a resonance (noted 1 in the figure (2)(a)) of the Poincaré section of the MPSW. Because of the large number of periods for this waveguide configuration, the high index segments are not superimposed on the field distribution in order to keep a clear picture (a). Husimi representation on figure (b), figure (c) represents the modal spectrum distribution which shows a large set of modes compared to figure 3 (c)) but they are still regularly spaced which is confirmed by the length spectrum shown in figure (d) that only exhibits the period of $584\mu m$ and its harmonics.

5. Comparison with the equivalent continuous waveguide model

Modes of PSW can be rigorously calculated with the help of Floquet-Bloch theorem which expresses the modes of the structure in terms of Spatial Harmonics (SH) [38, 39] or using modal method of diffraction grating [40]. Both methods remain efficient even in the case of a high index contrast between the segments and the substrate. Thus, an eigenfunction of a PSW is formally a Bloch function. Nevertheless, it has been shown that the simple

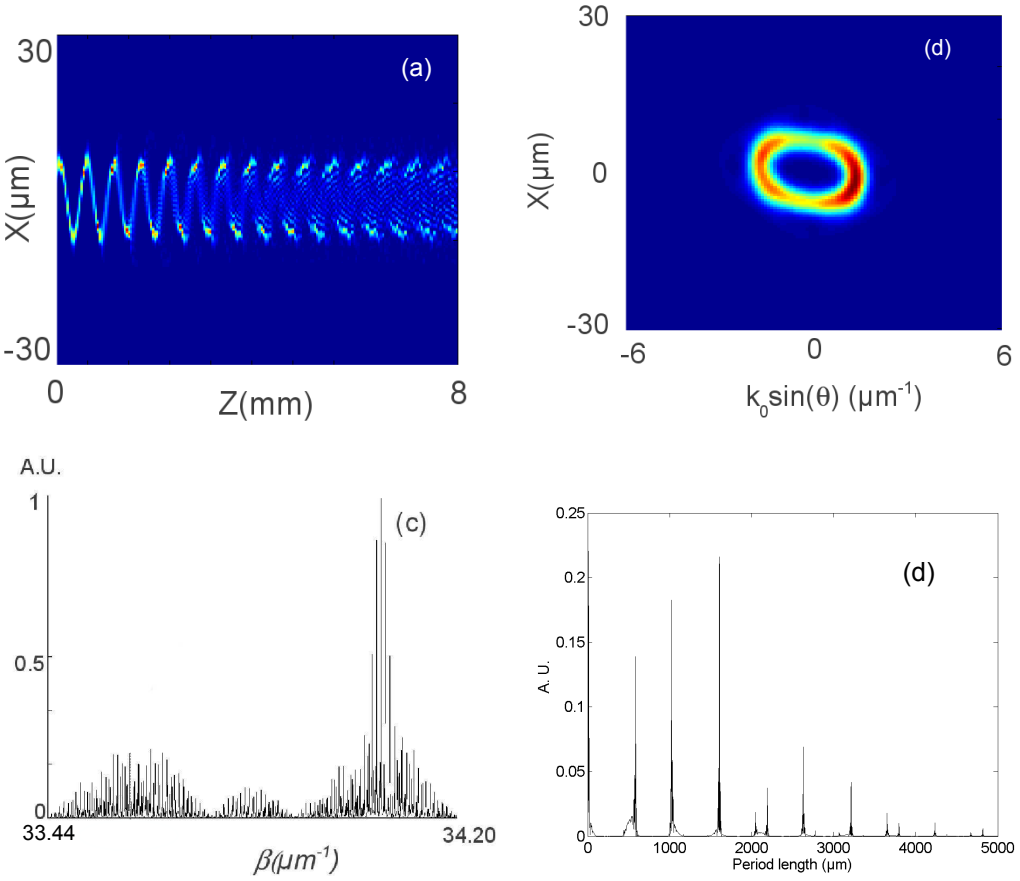

Fig. 6. Field distribution for an incident gaussian beam launched outside of a resonance (noted 2 in the figure (2)(a)) of the Poincaré section of the MPSW (a), Husimi representation (b). On figure (c) it is represented the modal spectrum distribution which shows a large set of modes but, unlike the previous case, modes are not regularly spaced as it can be seen with figure (d) where the Fourier transform of the spectrum exhibits a non harmonic distribution of periods length

equivalent continuous waveguide model (ECWM) constitutes a good approximation of a PSW. ECWG model has been widely used with success in many PSW device design [1, 2, 5–7, 11, 29] and validated by different approaches [32, 33, 40, 41]. The refractive index of the ECWG n_{eq} is the weighted average of the index of the PSW along the propagation direction and is given by :

$$\delta_{neq} = DC \times \delta n \tag{8}$$

This assumption strongly simplifies modes calculation for a PSW. The variation of the index of refraction along the propagation is then removed and the problem is reduced to a transverse waveguide modes calculation. In the case of uniform waveguide approximation, the

general solutions can be expressed as the transverse normal-mode eigenfunction expansions :

$$E(x,z) = \sum_n A_n u_n(x) exp(-i\beta_n z) \tag{9}$$

where A_n is the mode amplitude of the mode n, $u_n(x)$ is the transverse mode profile and β_n is the propagation constant of the mode n. Then, using a standard modes solver, it is easy to get the modal spectrum of the ECWM. The total modal distribution of the ECWG associated with the MPSW defined in section 2 is given in figure 7 for the two waveguide configuration and propagation constants are compared to the modal distribution of a MPSW obtained previously in the case of a collimated beams propagation. The β values of MPSW excited modes do not correspond to β values of the ECWG for both waveguides configurations and this means that the use of the equivalent waveguide model for the β calculation is no longer valid in the case of chaotic MPSW. Previous work based on ray dispersion has already mentioned that this feature may occur in MPSW [14] and strong deviations of the ECWG model has already been predicted. The ECWG mode based on a refractive index average cannot take into account the complexity of the dynamics which comes from the transverse index profile combined with the periodicity in the direction of the propagation.
Furthermore, it is interesting to nentionned that a regularly spaced spectral distribution that occurs here in the case of collimated beams propagation corresponds to a well known characteristic property of parabolic index continuous waveguides.

6. Conclusion

In this article, light propagation in a MPSW that exhibits a chaotic dynamics in the classical ray approach, has been investigated with the help of a modal analysis. Depending on initials conditions, light can follow a *snake like* propagating pattern all along the waveguide or may be spread over the entire cross section of the waveguide. The modal analysis revels that the *snake like* propagation is due to a superposition of specific regularly spaced eigenmodes of the MPSW. The beating length L_c of adjacent modes given by $L_c = \frac{\pi}{|\beta_i - \beta_{i+1}|}$ is then commensurable with the period Λ of segmentation of the waveguide. The modal analysis highlights also that the values of propagation constants of a MPSW do not matched with those obtained for the ECWG. Therefore, the widely used ECWG model is no longer valid in the case of a chaotic MPSW.

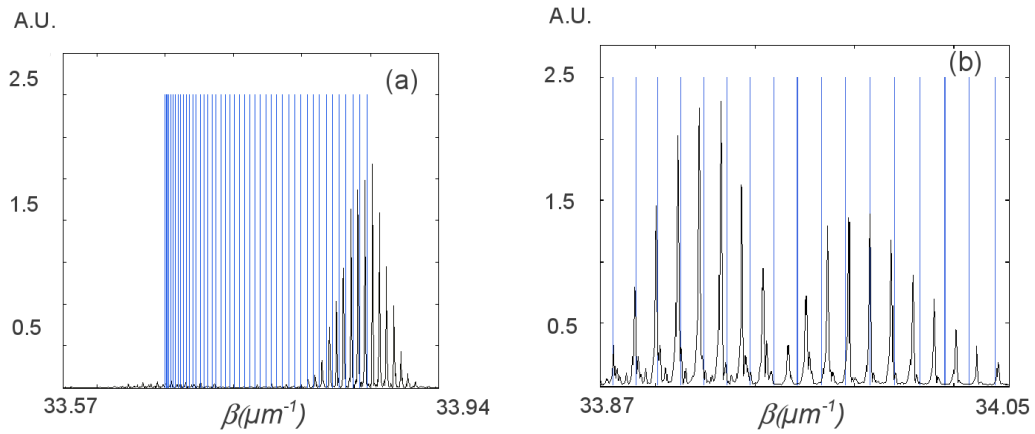

Fig. 7. Total modal spectrum of the ECWG (in blue) and the modes excited when an incident gaussian beam is launched in a resonance of the Poincaré section (a) for the first waveguide configuration. The distribution of the excited modes of the MPSW does not match with the modal distribution of the ECWG. In figure (b), due to a larger number of modes and in order to have a clear picture, it is compared only one part of the spectrum of the ECWG and modes excited when an incident gaussian beam is launched in a resonance. The mismatched is still present.

Besides a merely academic interest, the coexistence of collimated and dispersed regimes of light propagation in a waveguide could be of interest in the field of integrated optics.

References

[1] Z. Weissman and A. Hardy, "2-D mode tapering via tapered channel waveguide segmentation," Electron. Lett **28**, 1514–1516 (1992).

[2] Z. Weissman and I. Hendel, "Analysis of periodically segmented waveguide mode expanders," J. Lightwave Technol. **13**, 2053–2058 (1995).

[3] M. M. Spuhler, B. Offrein, G. Bona, R. Germann, I. Massarek, and D. Ern, "A very short planar silica spot-size converter using a nonperiodic segmented waveguide," J. Lightwave Technol. **16**, 1680 (1998).

[4] F. Dorgeuille, B. Mersali, S. Francois, G. Herve-Gruyer, and M. Filoche, "Spot size transformer with a periodically segmented waveguide based on InP," Opt. Lett. **20**, 581–583 (1995).

[5] M. H. Chou, M. A. Arbore, and M. M. Fejer, "Adiabatically tapered periodic segmentation of channel waveguides for mode-size transformation and fundamental mode excitation," Opt.

Lett. **21**, 794–796 (1996).

[6] D. Castaldini, P. Bassi, P. Aschiéri, S. Tascu, M. D. Micheli, and P. A. Baldi, "High performance mode adapters based on segmented SPE:LiNbO3 waveguides," Opt. Express **17**, 17868–17873 (2009).

[7] D. Castaldini, P. Bassi, S. Tascu, P. Aschiéri, M. P. D. Micheli, and P. Baldi, "Soft-Proton-Exchange tapers for low insertion-loss LiNbO3 devices," J. Lightwave Technol. **25**, 1588–1593 (2007).

[8] P. Aschiéri and M. P. de Micheli, "Highly efficient coupling in lithium niobate photonic wires by the use of a segmented waveguide coupler," Appl. Opt. **50**, 3885–3888 (2011).

[9] J. D. Bierlein, D. B. Laubacher, J. B. Brown, and C. J. van der Poel, "Balanced phase matching in KTiOP4 waveguides," Appl. Phys. Lett. **56**, 1725–1727 (1990).

[10] Z. Weissman, A. Hardy, M. Katz, M. Oron, and D. Eger, "Second-harmonic generation in Bragg-resonant quasi-phase-matched periodically segmented waveguides," Opt. Lett. **20**, 674–676 (1995).

[11] M. Sundheimer, P. Aschieri, P. Baldi, and J. Bierlein, "Modeling and experimental observation of parametric processes in segmented KTiOPO4 channel waveguides," Appl. Phys. Lett. **74**, 1660–1662 (1999).

[12] P. Aschiéri, F. Fogli, P. Aumont, M. D. Micheli, G. Bellanca, and P. Bassi, "Optical power management using second harmonic generation in periodic segmented waveguides," Opt. Commun. **235**, 55–61 (2004).

[13] P. Aschiéri, V. Doya, and A. Picozzi, "Complex behaviour of a ray in a gaussian index profile periodically segmented waveguide," J. Opt. A: Pure Appl. Opt **8**, 386–390 (2006).

[14] P. Aschiéri and V. Doya, "Ray dispersion strongly modified by a periodic index segmentation," Opt. Commun. **283**, 3673–3677 (2010).

[15] J. U. Nockel and A. D. Stone, "Ray and wave chaos in asymmetric resonant optical cavities," Nature **385**, 45–47 (1997).

[16] T. Gensty, K. Becker, I. Fischer, W. Elsäßer, C. Degen, P. Debernardi, and G. P. Bava, "Wave chaos in real-world Vertical-Cavity Surface-Emitting Lasers," Phys. Rev. Lett. **94**, 233901 (2005).

[17] J. Dingjan, E. Altewischer, M. P. van Exter, and J. P. Woerdman, "Experimental observation of wave chaos in a conventional optical resonator," Phys. Rev. Lett. **88**, 064101 (2002).

[18] S. Shinohara and T. Harayama, "Signature of ray chaos in quasibound wave functions for a stadium-shaped dielectric cavity," Phys. Rev. E **75**, 036216 (2007).

[19] M. Hentschel and K. Richter, "Quantum chaos in optical systems: The annular billiard," Phys. Rev. E **66**, 056207 (2002).

[20] W. Fang, A. Yamilov, and H. Cao, "Analysis of high-quality modes in open chaotic microcavities," Phys. Rev. A **72**, 023815 (2005).

[21] S.-Y. Lee, S. Rim, J.-W. Ryu, T.-Y. Kwon, M. Choi, and C.-M. Kim, "Quasiscarred resonances in a spiral-shaped microcavity," Phys. Rev. Lett. **93**, 164102 (2004).

[22] M. Lebental, J. S. Lauret, R. Hierle, and J. Zyss, "Highly directional stadium-shaped polymer microlasers," Appl. Phys. Lett. **88**, 031108 (2006).

[23] N. Djellali, I. Gozhyk, D. Owens, S. Lozenko, M. Lebental, J. Lautru, C. Ulysse, B. Kippelen, and J. Zyss, "Controlling the directional emission of holey organic microlasers," Appl. Phys. Lett. **95**, 101108 (2009).

[24] V. Doya, O. Legrand, F. Mortessagne, and C. Miniatura, "Light scarring in an optical fiber," Phys. Rev. Lett. **88**, 014102 (2001).

[25] V. Doya, O. Legrand, and F. Mortessagne, "Optimized absorption in a chaotic double-clad fiber amplifier," Opt. Lett. **26**, 872–874 (2001).

[26] O. Bendix, J. Méndez-Bermúdez, G. Luna-Acosta, U. Kuhl, and H.-J. Stöckmann, "Design of beam splitters and microlasers using chaotic waveguides," Microelectron. J. **36**, 285–288 (2005). Low Dimensional Structures and Devices Conference.

[27] E. D. Leonel, "Corrugated waveguide under scaling investigation," Phys. Rev. Lett. **98**, 114102 (2007).

[28] P. Aschiéri and V. Doya, "Unexpected light behaviour in periodic segmented waveguides," Chaos: An Interdisciplinary Journal of Nonlinear Science **21**, 043118 (2011).

[29] D. Ortega, R. M. D. L. Rue, and J. S. Aitchison, "Cutoff wavelength of periodically segmented waveguides in Ti:LiNbO3," J. Lightwave Technol. **16**, 284 (1998).

[30] M. De Micheli, J. Botineau, S. Neveu, P. Sibillot, and D. B. Ostrowsky, "Independent control of index and profile in proton-exchanged lithium niobate guide," Opt. Lett. **8**, 114–115 (1983).

[31] J. Vollmer, J. P. Nisius, P. Hertel, and E. Krtzig, "Refractive index profiles of LiNbO3: Ti waveguides," Applied Physics A **32**, 125–127 (1983).

[32] V. Rastogi, A. K. Ghatak, D. B. Ostrowsky, K. Thyagarajan, and M. R. Shenoy, "Ray analysis

of parabolic-index segmented planar waveguide," Appl. Opt. **37**, 4851–4856 (1998).

[33] V. Mahalakshmi, K. Thyagarajan, and M. R. Shenoy, "Propagation characteristics of planar segmented waveguides with parabolic index segments," Opt. Lett. **19**, 2113 (1994).

[34] A. Ghatak and K. Thyagarajan, *Introduction to fiber optics* (Cambridge University Press, 1998).

[35] Z. Weissman and A. Hardy, "Modes of periodically segmented waveguides," J. Lightwave Technol. **11**, 1831–1838 (1993).

[36] M. D. Feit and J. J. A. Fleck, "Computation of mode properties in optical fiber waveguides by a propagating beam method," Appl. Opt. **19**, 1154–1164 (1980).

[37] K. Husimi, "Some formal properties of the density matrix," Math. Soc. Jpn. **22**, 264–314 (1940).

[38] F. Fogli, N. Greco, P. Bassi, G. Bellanca, P. Aschieri, and P. Baldi, "Spatial harmonics modelling of planar periodic segmented waveguides," Optical and Quantum Electronics **33**, 485–498 (2001).

[39] F. Fogli, G. Bellanca, P. Aschieri, M. D. Micheli, and P. Bassi, "Spatial harmonics analysis of deep waveguide Bragg gratings," J. Opt. A: Pure Appl. Opt. **6**, 433–438 (2004).

[40] L. Li and J. Burke, "Linear propagation characteristics of periodically segmented waveguides," Opt. Lett. **17**, 1195–1197 (1992).

[41] D. Stancil, "Kronig-Penny model for periodically segmented waveguides," Appl. Opt. **35**, 4767 (1996).